Defining erosion limit for concrete

by

Bibiana M. Luccioni, Gabriel F. Aráoz and Nicolás A. Labanda

Reprinted from
International Journal of
Protective Structures

Volume 4 · Number 3 · September 2013

Multi-Science Publishing
ISSN 2041-4196

Defining Erosion Limit for Concrete

Bibiana M. Luccioni[a,b], Gabriel F. Aráoz[b] and Nicolás A. Labanda[a,b]
[a]CONICET, [b]Structures Institute, National University of Tucumán, Av. Independencia 1800, San Miguel de Tucumán, Argentina

Received on 6 April 2013, Accepted on 20 May 2013

ABSTRACT
Numerical simulation is usually used for predicting the response of concrete and fiber reinforced concrete structures to blast or impact loads. Depending on both charge weight and standoff distance, blast loads can cause fracture and spalling of concrete. In order to numerically reproduce these effects, an erosion model can be used to remove from the calculation the elements that have reached certain criteria. This erosion model represents a numerical tool to avoid great distortion of Lagrange meshes. For this reason, its application to the simulation of a physical phenomenon requires the calibration with experimental results. A review of different erosion criteria and limits used by different authors to simulate concrete under blast loads is presented in this paper. Some application examples and comparisons with experimental results are developed to show the effect of erosion limit on damage results and the dependence on the materials properties, mesh size and scaled distance.

Key words: Blast, concrete, erosion, numerical simulation.

1. INTRODUCTION

The study of blast loads has become important during the last decades due to the large amount of accidental and intentional events occurring worldwide indicating the relevance of the topic in structural design and reliability analysis. Consequently, extensive investigations have been developed in the field of explosive charges during the last decades [1]. This research is important not only because it helps understanding the damage caused by explosions on structures and buildings but also because it allows predicting the blast vulnerability of structures and humans and developing new explosion resistant materials and protective structures [2].

Research in this area has been oriented toward two different targets [3]: protecting new or existing structures against possible blast attacks or, in cases of attacks already produced, inferring the characteristics of the blast load used (size, shape, position, etc.) [4–5]. Achieving the first objective involves minimizing the damage and preventing structural collapse against unknown loads which is practically impossible. In order to protect buildings that represent potential targets of attack the effort has generally been focused on limiting the approximation of vehicles that may carry explosives or building protective elements which somehow reduce the incident blast pressure on the structures [6]. In both cases it is important to understand and to be able to predict the behavior of structures and protective elements under blast loads.

*Corresponding author. E-mail address: bluccioni@herrera.unt.edu.ar

Concrete has been and is still being used extensively to construct civilian buildings, dams, nuclear reactor containments and various defense structures. Moreover, nowadays high and ultrahigh performance concrete including different types of fibers are emerging as promising materials for the construction of structures resistant to impact and explosions. Therefore, it is important to investigate the behavior of this type of materials under blast and impact loadings that cause large strains, high strain rates, spalling, fracture and crushing phenomena [7].

An explosion in contact or very close to a concrete element is likely to cause a localized shear failure before the wall or column has time to respond to loading in a flexural mode. Localized back face spalling can take place but a breach of the wall or the column could occur due to a shear failure [8]. An explosion at a small distance from a concrete wall will cause a high-speed pressure wave to the front face of the wall. Part of the blast wave energy will be reflected back and a significant proportion will propagate through the wall as a compressive stress wave. When this wave reaches the back face another reflection will take place leading to a tension rebound that can cause back face spalling. Concrete fails in tension and particles are ejected from the back surface at high speed [8]. An explosive loading originated from a greater standoff location could cause failure in flexure of the entire concrete section.

The different ways of structural failure are related to the different stress states that the material suffers inside the structure. Close to the explosive load the material is subjected to high hydrostatic pressures that produce the material irreversible compactation and stiffening. More distant, the confining pressures reduce and the material is subjected to moderated triaxial compression. Finally, the compression wave can be reflected originating a tension wave that interacts with compression waves producing fragmentation [9].

Although experimental research should always be carried out to understand the behavior of materials and structures, numerical simulation is usually used for predicting the response of these types of structures to blast or impact loads since experimental studies are usually expensive and time consuming. Hence, a lot of effort has been devoted to model the dynamic response of concrete and fiber reinforced concrete elements [7], [10–17]. Nevertheless, the simulation of concrete erosion and spalling still requires further research.

The development of hydrocodes makes possible the simulation of complete blast problems. Although hydrocodes can analyze problems with different types of processors: Lagrangian, Eulerian, SPH, solid structures are usually modeled using Lagrangian grids even though it is clear that the materials will be subjected to very large distortions. In explicit codes, severely crushed elements can lead to a very small time step, resulting in the use of many computational cycles with negligible advance in the simulation time. Moreover, Lagrangian elements which have become very distorted have a tendency to "lock up," thereby inducing unrealistic distortions in the computational mesh [18]. The element erosion function provides a numerical solution to these problems. Erosion is characterized by a physical separation of the eroded solid element from the rest of the mesh [19]. It constitutes an attractive tool to simulate the spalling of concrete and provides a more realistic graphical representation of the actual blast events. But, although element removal (erosion) associated with total element failure has the appearance of physical material erosion, it is, in fact, a numerical technique that allows the calculation to proceed.

Erosion function allows removing such Lagrangian cells from the calculation if a pre-defined criterion is reached. When a cell is removed from the calculation process, the mass within the cell can either be discarded or distributed to the corner nodes of the cell. If the mass is retained, conservation of inertia and spatial continuity of inertia are maintained. However, the compressive strength and internal energy of the material within the cell are lost

whether or not the mass is retained. Erosion causes losses of internal energy, strength and (possibly) mass, therefore erosion limits should be chosen so that cells are not discarded (eroded) until they are severely deformed and their compressive strength and/or mass are not likely to affect the overall results [20].

Code's manuals usually remark that, although erosion could be used to model actual material erosion it is not true modeling of a physical phenomena but a numerical solution to overcome problems associated with the excessive mesh distortions. In consequence, erosion criteria and limits should be carefully adjusted to reproduce experimental results. In absence of experimental evidence it is generally recommended to perform calculus with variable erosion limits to evaluate the effect of erosion limit on numerical results and to use limiting values as high as practicable. The problem is that comparison with existing experimental results show that when high erosion limits are used for concrete, reinforced concrete or fiber reinforced concrete elements under blast loads, the actual type of failure cannot be reproduced. On the other side, both for design and post blast charge evaluation, numerical simulation should be able to predict structural behavior without knowing actual response. If a test is needed for each situation the advantage of performing numerical simulations is lost.

The objective of this paper is the study of the erosion effect on the numerical solution of concrete elements under blast loads. First, different available erosion criteria are presented together with the values of erosion limits used by different authors for the numerical simulation of concrete elements under blast loads. Application examples and comparison with experimental results are presented to show the effect of using different erosion criteria and the variability of numerical results with erosion limit and mesh size. Moreover, it is proved that erosion limit based on strain values cannot be fixed independently of the mesh size.

2. EROSION MODELS

A summary of different erosion criteria and limits used for the numerical simulation of concrete that can be found in recent papers is included. Additionally, other techniques used to avoid using erosion are also mentioned in this section. The section is completed with some comments about the great dispersion in erosion values found in literature.

2.1. EROSION CRITERIA

The different erosion criteria available in the literature can be classified according to the type of variable used to control erosion.

21.1. Strain Based

Since erosion is basically a numerical tool to avoid great mesh distortions, criteria based on strain limits are widely used for defining erosion models. Normally, the static strain limits are incremented to take into account the strain rate effects.

2.1.1.1. Instantaneous geometric strain

Erosion is initiated when an instantaneous geometric strain limit is reached,

$$\varepsilon_{eff} \geq \left(\varepsilon_{eff}\right)_{\lim} \tag{1}$$

$$\varepsilon_{eff} = \frac{2}{3}\sqrt{\left(\varepsilon_1{}^2 + \varepsilon_2{}^2 + \varepsilon_3{}^2\right) + 5\left(\varepsilon_1\varepsilon_2 + \varepsilon_1\varepsilon_3 + \varepsilon_2\varepsilon_3\right) - 3\left(\varepsilon_{12}{}^2 + \varepsilon_{23}{}^2 + \varepsilon_{13}{}^2\right)} \tag{2}$$

This criterion represents a limit in effective strain, a kind of quadratic norm of the strain tensor. The instantaneous geometric strain can increase or decrease with loading and unloading but once an element has been eroded it can no longer be recovered. It should be noted that this criterion is independent of the strain sign. In this sense, it seems to be useful for metals but not adequate to model frictional materials response characterized by a great difference between tension and compression behavior. Nevertheless, this criterion has been used by some authors to model concrete and fiber reinforced concrete under blast loads [21] and impact load [13], [21–25]. Some of these authors distinguish between compression and tension limits [21–22], [24–26] but it is not clear how are effective compression strain and effective tension strain defined. Limit values used for compression are always higher than limit values for tension. In some cases only effective strain in compression is limited and in many cases the erosion limits used for compression are several orders higher than concrete compression strain at failure under high dynamic loads. As a consequence, concrete elements are eroded much after failure.

2.1.1.2. Maximum principal strain

Erosion is initiated when a maximum principal strain is reached,

$$\varepsilon_1 \geq \left(\varepsilon_1\right)_{\text{lim}} \tag{3}$$

The maximum strain can increase and decrease with loading and unloading but like in the preceding case, once the element has been eroded, it can no longer be recovered. This is typically a limit in tension strain. When applied to brittle materials like concrete it can be physically interpreted as a limit in crack opening. It can represent tensile fracture and spalling of concrete under blast and impact loads but it seems useless to represent brisance effect or erosion under high compression stresses.

This criterion has been used by many authors to represent concrete erosion under blast loads [27] [19] [28], concrete under high dynamic loads [12] and fiber reinforced concrete (FRC) under impact load [29]. The values used for the erosion limit in tension are sensible lower than those used for the instantaneous geometric strain and resemble concrete limit strain under tension. Xu and Lu [30] define the erosion by a limit tensile strain that they calculate from static tensile limit strain considering dynamic amplification under blast loads, effect of confinement and reinforcement. Using this approach, they obtain a good representation of the phenomenon of spallation of reinforced concrete plates. Nevertheless, they state that more robust criteria for erosion may result in more accurate simulations.

2.1.1.3. Maximum shear strain

Erosion is initiated when a maximum shear strain reaches a shear strain limit,

$$\gamma_1 \geq \left(\gamma_1\right)_{\text{lim}} \tag{4}$$

Like previous erosion limits, the maximum shear strain can increase or decrease with loading/unloading but once an element has been eroded it is eliminated from calculus and it cannot be recovered. This criterion can be physically assimilated to shear failure like that obtained in concrete elements subjected to contact explosions or close blast loads, or concrete plates under projectile perforation. In all these cases, the concrete element failure is

characterized by a local shear failure that takes place before the loads are transmitted to the supports and structural behavior is mobilized. The estimation of the shear strain erosion limit from concrete properties is not straightforward.

Many authors have used this criterion to define erosion of concrete [27] and FRC [31] under blast loads and projectile impact and erosion produced by projectile impact [25], [29], [32] and low velocity impact [33] on FRC plates.

2.1.1.4. Incremental geometric strain

Erosion is initiated when an incremental geometric strain limit is reached,

$$\overline{\varepsilon}_{eff} \geq \left(\overline{\varepsilon}_{eff}\right)_{\lim} \tag{5}$$

$$\overline{\varepsilon}_{eff} = \int \dot{\overline{\varepsilon}}_{eff} dt \qquad \dot{\overline{\varepsilon}}_{eff} = \frac{2}{3}\sqrt{\dot{\varepsilon}_{xx}^2+\dot{\varepsilon}_{yy}^2+\dot{\varepsilon}_{zz}^2+\dot{\varepsilon}_{xy}^2+\dot{\varepsilon}_{xz}^2+\dot{\varepsilon}_{yz}^2} \tag{6}$$

Incremental geometric strain is always an increasing measure of strains but it makes no difference between tension and compression strains. Additionally, it is difficult to relate it to a physical measure of strains to fix the limit. Although available in commercial codes [20], no papers using this type of erosion criterion have been found in the literature.

2.1.1.5. Effective plastic strain

Erosion is initiated when an effective plastic strain limit is reached [20],

$$\varepsilon_{eff}^{p} \geq \left(\varepsilon_{eff}^{p}\right)_{\lim} \tag{7}$$

$$\varepsilon_{eff}^{p} = \int \dot{\varepsilon}_{eff}^{p} dt \qquad \dot{\varepsilon}_{eff}^{p} = \frac{\sqrt{3J_2}-\sigma_y}{3G} \tag{8}$$

J_2: second invariant of the stress deviator
σ_y: uniaxial yield stress
G: shear modulus

This is a plasticity based criterion with the advantage that plastic strains are irreversible and can be physically interpreted as irrecoverably deformations. Eqn. (8) defines a J_2 plastic flow, normally used in hydrocodes where hydrostatic and deviatory responses are decoupled. Nevertheless, a more complex plastic flow can be used. Although it has physical foundations, no references using this type of erosion criterion for concrete under impact or blast loads have been found.

2.1.2. *Stress Based*

Stress based erosion criteria are similar to yield criteria in classical plasticity. The strength enhancement due to high strain rates should be taken into account in the stress-based erosion limits.

Different ways of defining the stress erosion limit can be found.

2.1.2.1. Pressure

Erosion is initiated when a maximum (minimum) pressure is reached,

$$p \geq p_{\lim} \text{ or } p \leq p_{\min} \tag{9}$$

When it is used in tension, this erosion criterion is similar to tension cut off in classical plasticity or hydro tensile limit. No references using this erosion limit have been found.

2.1.2.2. Principal stress

Erosion is initiated when maximum principal stress reaches a limit,

$$\sigma_1 \geq (\sigma_1)_{\lim} \tag{10}$$

This criterion can be physically assimilated to a limitation of tension stresses (tension cut off) and the values of the stress limit can be derived from tension strength of concrete. It has been used to model concrete [28] and FRC [31] under blast loads and FRC under projectile impact [31–32].

2.1.2.3. Effective stress

Erosion is initiated when the effective stress reaches a limit,

$$\sigma_{eff} \geq (\sigma_{eff})_{\lim} \tag{11}$$

$$\sigma_{eff} = \sqrt{\frac{2}{3}\sigma_{ij}\sigma_{ij}} \tag{12}$$

This is a typically J_2 based criterion for metallic materials. Although available in hydro codes it is no suitable for frictional materials like concrete.

2.1.3. Damage Based

Erosion is initiated when damage limit is reached,

$$D \geq (D)_{\lim} \tag{13}$$

This criterion seems to be adequate and physically founded. Damage used as erosion indicator is an always increasing variable, generally associated with stiffness degradation. Nevertheless, it should be noted that this type of criteria is strongly related to the constitutive model used for concrete. A model considering damage should be used and depending on the type of damage model, different definitions of the damage variable and its evolution can be found.

Zhou *et al*. [14] have used a tensile damage criterion to model concrete under blast loads using a micro mechanical approach. Cuoghlin *et al*. [34] used a damage criterion to model erosion in FRC under impact loads.

2.1.4. Failure

All the preceding erosion criteria can be considered as failure criteria. Other failure criteria that are available in commercial codes to define erosion are presented in this section. No use of this type of criteria has been found in the specialized literature.

Failure [20]: Erosion is initiated after element failure. For example when Tuler-Butcher criterion [35] is reached,

$$\int_0^t \left[\max(0, \sigma_1 - \sigma_0)\right]^2 dt \geq K_f \tag{14}$$

σ_o is a specified threshold stress
K_f is the stress impulse at failure

2.1.5. Other

Erosion is initiated when a minimum element timestep [20] is reached,

$$\Delta t \leq \Delta t_{\text{lim}} \tag{15}$$

This type of criterion has numerical meaning but it is difficult to relate to the material physics.

2.1.6. Summary of Erosion Criteria and Limits Used by Different Authors

The erosion criteria and limit values used by different authors in recent papers to simulate concrete, reinforced concrete (RC), fiber reinforced concrete (FRC) and high performance fiber reinforced concrete (HPFRC) under blast loads are summarized in Table 1 where the corresponding references are also included.

2.2. ALTERNATIVE PROCEDURES

To avoid using erosion technique, Wang *et al*. [31] presented a method based on continuum damage mechanics and mechanics of micro-crack development. The fragmentation process was modeled according to the crack initiation and propagation, which depend on the material damage levels.

Alternatively, Riedel *et al*. [15] stopped the simulation when the damage was fully established but when the damaged material was still mostly in place. Cells extremely damaged were deleted in problem visualization showing the same aspect to that achieved with erosion criteria and avoiding too long simulations.

All the works mentioned in previous sections and above were conducted with finite element method (FEM), in which erosion method must be implemented to delete some elements and capture the perforation phenomenon. Meshfree/meshless and particle methods are alternative methods to handle this problem that have received considerable attention during last decades [7]. A representative of such methods is the material point method (MPM), which is an extension of the fluid implicit particle (FLIP) method to solid mechanics. MPM discretizes a material domain by a set of Lagrangian material points (particles) moving through an Eulerian background grid. The numerical dissipation normally associated with Eulerian methods is removed, while mesh distortion and element entanglement associated with the Lagrangian finite element method are avoided [7].

Table 1. Different erosion criteria and erosion limits used in recent papers.

Scaled distance [m/kg$^{1/3}$]	Problem	Material	Mesh size [mm]	Criteria	Limit	Reference
0.12-0.29	RC plate	Concrete 40 MPa	18.75×18.75 x25	Principal strain	0.01	[30]
1	RC wall	Concrete 35 Mpa	12 × 12 × 6 6 × 6 × 6	Instantaneous Geometric strain	–2	[21]
0.04 Contact explosion	Concrete plate	Concrete 48 MPa	2	Tensile damage and-effective strain or effective strain	0.99 0.2 2	[14]
1	RC frame	Concrete 24 MPa	50	Principal strain or Shear strain	0.15 0.9	[27]
0.05	RC bridge structures	Concrete 60 MPa	6.25	Tensile Stress and/or Principal strain	5 MPa 0.1	[28]
Contact explosion	Composite concrete/ steel column	Concrete 40 MPa	50	Principal tensile strain	0.1	[19]
0.23-2.5	RC plate	Concrete		Principal tensile strain	0.01	[16]
0.488-0.684	RC plate	Concrete 39.5 Pa	3			[17]
Contact explos.	FRC cylinder	FRC 1% 28 MPa		Shear strain or Tensile Stress	0.4 5.4 MPa	[31]
Contact explos.	FRC cylinder	FRC 1.5% 30 Mpa		Shear strain or Tensile Stress	0.4 6.0 MPa	[31]
Contact explos.	FRC cylinder	FRC 2% 32 MPa		Shear strain or Tensile Stress	0.4 7.5 MPa	[31]
— — —	FRC barriers	FRC 45 MPa	25 × 25	Damage	0.99	[34]

2.3 REMARKS

Numerous criteria have been used to simulate different types of concrete elements under explosive and impact loads. Additionally, some authors simultaneously used two erosion criteria so that the one that is first reached activates erosion. It is difficult to state which is the best erosion criterion from the summary of results presented in Section 2.1.6. It seems that erosion criteria should be appropriate to reproduce the type of failure expected.

Commercial software usually recommends the calibration with experimental results and the use of as high as possible erosion limits, but it is clear that this suggestion that could be useful for metals cannot be used to properly model concrete. It can be proved that different solutions are obtained for different erosion limits. Failure type can change from a local shear failure to a flexural failure when erosion limits are increased. Moreover, the fragility curve determination for an extreme damage level (collapse) was described by Aráoz and Luccioni [36] from a numerical analysis of masonry walls under blast loads considering the uncertainty of the material erosion limit. The important variability observed in the results obtained showed the importance and need of further research relative to erosion criteria and limits. These results and conclusion can be extrapolated to concrete.

Generally, all authors have calibrated erosion limits to reproduce the experimental results that correspond to different physical problems: contact blast, near field blast, distant blast, projectile impact, low velocity impact, etc. They show good results for the problems simulated. Most criteria are based on strain limits. The limit values used by different authors (Table 1) are extremely different even for similar material properties and mesh sizes.

On the other side, criteria based on strains limits normally assume that material undergoes softening up to certain strain limit. It is well known that stress-strain response is not a material property for materials undergoing softening. The independence of the mesh size should be checked when strain based erosion criteria are used in combination with finite element method. Authors usually adjust materials properties with experimental results and then use the corresponding properties to solve other problems. Nevertheless, it should be proved if that erosion limit is a material property independent of the mesh size.

Moreover, it is well known that in the case of blast loads concrete stress-strain response is strongly dependent on strain rate. Both strain and stress based erosion criteria should take into account strain rate effects on erosion limits. Some authors have mentioned these effects but it is not easy to a priori define one limit since strain rate is not previously known and is surely variable inside the structure.

Concluding, the question is how to decide the best erosion criterion and limit in order to simulate a certain problem whose type of failure is not previously known. That is usually the situation when designing protective elements or assessing damage due to blast loads to infer the location and amount of explosive used in an attack.

3. APPLICACTION EXAMPLES

3.1. INTRODUCTION

The study of the effect of erosion criterion and limits on the numerical results is developed in this section based on applications related to concrete, reinforced concrete and fiber reinforced concrete elements subjected to blast loads at different scaled distances.

All the numerical analysis is performed with the hydrocode ANSYS Autodyn [20]. An Euler Godunov multi material with strength higher order processor is used to model the air and the explosive while a Lagrange processor is used for concrete. In the case of contact explosions the complete problem is simulated with only one model. Two independent simulations are performed when the explosive is located at a certain standoff distance. First, the detonation of the explosive load is simulated in a smaller and more refined model using and Euler Godunov multi material processor and then, the results are mapped on a second model representing the structural element and the surrounding air volume. In this second model an Euler FCT processor is used for air.

The ideal gas equation of state is used for the air. Lee-Tarver equation of state [37] is used to model both the detonation and expansion of TNT in conjunction with "Jones - Wilkins - Lee" (JWL EOS) to model the unreacted explosive.

A RHT model [38] with a P-alpha equation of state [39] is used for concrete. The equation of state of the fully compacted or solid material is described with a polynomial function as,

$$p = A_1\ \mu + A_2\ \mu^2 + A_3\ \mu^3 + \left(B_0 + B_1\ \mu\right)\ \rho_0\ e \text{ for } p \geq 0 \text{ (compactation)}$$

$$p = T_1\ \mu + T_2\ \mu^2 + B_0\ \rho_0\ e \text{ for } p < 0 \tag{16}$$

where A_i, B_i and T_i are coefficients, ρ_0 is the initial density and

$$\mu = \frac{\rho}{\rho_0} - 1 \tag{17}$$

is the relative volume change.

The EOS for the porous material is calculated by substituting a new variable $\alpha\rho_p$ for ρ in eqn. (17) and eqn. (16), i.e.,

$$p = A_1\ \bar{\mu} + A_2\ \bar{\mu}^2 + A_3\ \bar{\mu}^3 + \left(B_0 + B_1\ \bar{\mu}\right)\ \rho_0\ e \text{ for } p \geq 0 \tag{18}$$

$$\bar{\mu} = \frac{\alpha\rho_p}{\rho_0} - 1 \tag{19}$$

where ρ_p is the density of the porous material and α a is called material "porosity" that can be defined as

$$\alpha = \frac{\rho_s}{\rho_p} \tag{20}$$

where ρ_s and ρ_p refer to the density of the solid and the porous material at the same pressure and temperature respectively . In the p-α equation of state the following definition is used,

$$\alpha(p) = 1 + \left(\alpha_{init} - 1\right)\ \left(\frac{p_{lock} - p}{p_{lock} - p_{crush}}\right)^n \tag{21}$$

where α_{init} is the initial porosity of the intact concrete; p_{crush} corresponds to the pore collapse pressure beyond which concrete plastic compaction occurs; p_{lock} is the pressure at which the concrete porosity α reaches unity and n is the compactation exponent.

The RHT strength model [38] is a combined plasticity and shear damage model in which the deviatoric stress $Y = \sqrt{3J_2}$ is limited by a generalized failure surface defined as

$$\left(\sqrt{3J_2}\right)_{fail} = Y_{fail}\left(p^*, \theta, \dot{\varepsilon}\right) = Y_C\left(p^*\right)\, r_3(\theta)\, F_{rate}\left(\dot{\varepsilon}\right) \tag{22}$$

$$Y_c\left(p^*\right) = f_c\left[A\,\left(p^* - p^*_{spall}\, F_{rate}\left(\dot{\varepsilon}\right)\right)^N\right] \tag{23}$$

Where f_c is the uniaxial compression strength; A and N are material constants; $p^* = p/f_c$ is the normalizad pressure, p is the hydrostatic pressure and $p^*_{spall} = f_t/f_c$, where f_t is the uniaxial tension strength; $F_{rate}(\dot{\varepsilon})$ represents the dynamic amplification factor (DIF) as a function of strain rate $\dot{\varepsilon}$.

$$r_3(\theta) = \frac{r}{r_c} \tag{24}$$

$$r_3(\theta) = \frac{2\left(1-\psi^2\right)\cos\theta + \left(2\psi - 1\right)\sqrt{4\left(1-\psi^2\right)\cos^2\theta + 5\psi^2 - 4\psi}}{4\left(1-\psi^2\right)\cos^2\theta + \left(1-2\psi\right)^2} \tag{25}$$

$$\cos 3\theta = \frac{3\sqrt{3}}{2}\frac{J_3}{\left(J_2\right)^{3/2}} \tag{26}$$

$$\psi = \frac{r_t}{r_c} = Q + BQp^* \tag{27}$$

J_2 and J_3 represent the second and the third invariants of the deviatoric stress tensor. The input parameter Q defines the ratio of strength at zero pressure and the coefficient BQ defines the rate at which the fracture surface transitions from an approximately triangular form to a circular form with increasing pressure.

Strain rate effects are represented through increases in fracture strength with plastic strain rate. Two different terms can be used for compression and tension with linear interpolation being used in the intermediate pressure regime.

$$F_{Rate} = \begin{cases} 1 + \left(\dfrac{\dot{\varepsilon}}{\dot{\varepsilon}_0}\right)^{\alpha} & for\ p > \frac{1}{3} f_c \ \text{(compression)} \\ 1 + \left(\dfrac{\dot{\varepsilon}}{\dot{\varepsilon}_0}\right)^{\delta} & for\ p < \frac{1}{3} f_t \ \text{(tension)} \end{cases} \tag{28}$$

δ is the compression strain rate factor; α is the tension strain rate factor and $\dot{\varepsilon}_0 = 3E - 6$ in tension and $30E - 6$ in compression.

Strain hardening is represented in the model through the definition of an elastic limit surface and a "hardening" slope. The elastic limit surface is scaled down from the fracture surface

$$Y_{elast} = Y_{fail}\left(p^{*}\right) F_{elast}\ F_{cap}\left(p\right) \tag{29}$$

F_{elas} is the ratio of the elastic strength to failure surface strength derived from two input parameters (elastic strength$/f_c$) and (elastic strength$/f_t$) and F_{cap} is a function that limits deviatoric stresses under hydrostatic compression [20]. The pre-peak fracture surface is defined by interpolation between the elastic and fracture surfaces using the "hardening" slope,

$$\frac{G_{elas}}{G_{elas} - G_{plas}} \tag{30}$$

The model presents the option of including a cap to limit the elastic deviatoric stress under large compressions. This option effectively leads to the assumption that porous compaction results in a reduction in deviatoric strength.

A residual (frictional) failure surface is defined as,

$$Y^{*}_{resid} = B\ p^{*M} \tag{31}$$

where B is the residual failure surface constant and M is the residual failure surface exponent, both input parameters.

Damage is assumed to accumulate due to inelastic deviatoric straining (shear induced cracking) using the relationships

$$D = \sum \frac{\Delta \varepsilon^{p}}{\varepsilon^{p}_{fail}}$$
$$\varepsilon^{p}_{fail} = D_1 (p* - p*_{spall})^{D_2} \tag{32}$$

where D_1 and D_2 are material constants used to describe the effect strain to fracture as a function of pressure.

Damage accumulation can have two effects in the model:

- Strain softening (reduction in strength). The current fracture surface (for a given level of damage) is scaled down from the intact surface,

$$Y^{*}_{fract} = (1-D)Y^{*}_{fail} + DY^{*}_{resid} \tag{33}$$

- Reduction in shear stiffness,

$$G_{frac} + (1-D)G_{elas} + DG_{resid} \tag{34}$$

RHT model allows the use of a principal stress failure criterion with linear strain softening defined by fracture energy.

Erosion criteria based on stress limits are not available in AUTODYN. In order to define erosion based on a principal stress limit, a tensile failure based on principal stress together with failure based criterion for erosion were used. In this case, elements are eroded when the principal stress reaches the stress limit before strain softening can take place. The eroded zone is coincident with the failed elements.

3.2. CONCRETE PLATE UNDER CONTACT BLAST LOAD (11)

A concrete slab tested under blast loading by Rabzuk and Eibl [11] was modeled. This slab has also been modeled by Zhou *et al.* [14]. The dimensions of the tested slab are 1.2 m × 1.2 m × 0.32 m. Parameters used to model concrete are presented in Table 2. The slab was supported at its corners and loaded by an explosive cone of TNT and Composition B. The equivalent charge weight was about 350 g. The inner cone consisted of TNT and the outer thin cone of composition B. A scheme of the tested slab with the dimensions in mm is shown in Figure 1. More details about this experimental test can be found in the paper by Rabzuk and Eibl [11].

The numerical model used to simulate this problem is represented in Figure 2. Due to symmetry conditions, only one fourth of the slab was actually modeled. The model contained the air volume where the slab was immersed and where the explosive was detonated and the slab itself. As the explosive was in contact with the slab the mesh was refined in coincidence with explosive charge to guarantee a minimum of ten elements inside explosive in each direction. Initially, a 2 mm cell size was used for the slab.

Air flow was allowed in the air mesh sides and the slab was supposed to be fixed in its corners. Euler-Lagrange interaction was defined.

The problem was run until no more deformation or erosion occurs.

The material properties used are presented in Table 2.

Instantaneous geometric strain was first used as erosion criterion. Following the usual recommendations, erosion limit was varied in order to obtain a numerical solution that correlates to experimental results in terms of physical erosion. Figure 3 shows the damage obtained with a 2 mm cell size for different erosion limits. The dimensions of the slab perforation obtained are presented in Table 3 together with experimental results [11]. From Figure 3 and Table 3 it is clear that in this case the more appropriate value for the erosion geometric strain limit is 0.001.

In order to study the relation between the erosion limit and the mesh size the same problem was solved but with a coarser mesh (10 mm). As done for the finer mesh, erosion limit value was varied in order to obtain the damage pattern observed in the test [11]. The corresponding damage patterns and crater diameters were compared with experimental results. It seems that actual damage was better modeled with an erosion limit of 0.0002. The corresponding results are presented in Figure 4 and Table 3. This erosion value can be obtained based on an analogy with the procedure used to obtain mesh size objectivity when finite element method is used in combination with strain softening models. Nevertheless, it should be noted that for this value the crater was rather bigger than the crater found in the experiment [11].

If an even coarser mesh is used, the erosion limit should be corrected to obtain the same damage pattern but it is difficult to reproduce physical erosion with a coarse mesh. It should be observed that damage pattern is strongly dependent not only on erosion limit but also on mesh size. Moreover, strain based erosion limits are not independent of mesh size.

In order to analyze the behavior of different erosion criteria, the same problem was solved but with other erosion criteria. The results are compared with those previously obtained and with experimental results.

Table 2. Concrete properties

	Application example section				
Equation of State P alpha	**3.2 Concrete**	**3.3 Concrete**	**3.4 Concrete**	**3.5 Concrete**	**3.5 UHPFC**
Reference density (g/cm^3)	2.75	2.75	2.75	2.75	2.75
Porous density (g/cm^3)	2.33	2.33	2.33	2.33	2.33
Initial compaction pres (kPa)	2.4E+4	2.4E+4	2.4E+4	2.4E+4	2.4E+4
Solid compaction pres (kPa)	2.5E+5	2.5E+5	2.5E+5	2.5E+5	2.5E+5
Compaction exponent *n*	3.0	3.0	3.0	3.0	3.0
Solid EOS	Polynom	Polynom	Polynom	Polynom	Polynom
Bulk Modulus A1 (kPa)	3.53E+7	3.53E+7	2.076+7	2.076E+7	3.45E+7
Parameter A2 (kPa)	3.96E+7	3.96E+7	3.96E+7	3.96E+7	3.96E+7
Parameter A3 (kPa)	9.04E+6	9.04E+6	9.04E+6	9.04E+6	9.04E+6
Parameter B0	1.22	1.22	1.22	1.22	1.22
Parameter B1	1.22	1.22	1.22	1.22	1.22
Parameter T1 (kPa)	3.53E7	3.53E7	3.53E7	3.53E7	3.53E7
Parameter T2 (kPa)	0.00	0.00	0.00	0.00	0.00
Compaction Curve	Standard	Standard	Standard	Standard	Standard
Strength (RHT Concrete)					
Shear modulus (G) (kPa)	1.5E+7	2.0E+7	1.18E+7	1.18E+7	1.96E+7
Compres Strength (f_c) (kPa)	4.8E+4	4.8E+4	3.95E+4	3.95E+4	15.16E+4
Tensile Strength (f_t/f_c)	8.33E-02	1.10E-01	1.10E-01	1.10E-01	2.0E-01
Shear Strength (f_s/f_c)	1.80E-01	1.80E-01	1.80E-01	1.80E-01	3.50E-01
Intact Failure Surf Constant A	1.60	1.60	1.60	1.60	1.60
Intact Failure Surf Expon. N	6.10E-01	6.10E-01	6.10E-01	6.10E-01	6.10E-01
Tens./Comp. Merid Ratio (Q)	6.805E-1	6.805E-1	6.805E-1	6.805E-1	6.805E-1
Brittle to Ductile Transition	1.05E-02	1.05E-02	1.05E-02	1.05E-02	1.05E-02
G (elas.)/(elas.-plas.)	2.00	2.00	2.00	2.00	2.00
Elastic Strength / f_t	7.00E-01	7.00E-01	7.00E-01	7.00E-01	7.00E-01
Elastic Strength / f_c	5.30E-01	5.30E-01	5.30E-01	5.30E-01	5.30E-01
Frac Strength Constant B	1.60	1.60	1.60	1.60	1.60
Frac Strength Exponent M	6.10E-01	6.10E-01	6.10E-01	6.10E-01	6.10E-01
Compres Strain Rate Exp. α	3.20E-02	3.20E-02	3.20E-02	3.20E-02	3.20E-02
Tensile Strain Rate Exp. δ	3.60E-02	3.60E-02	3.60E-02	3.60E-02	3.60E-02
Use CAP on Elastic Surface?	Yes	Yes	Yes	Yes	Yes
Failure RHT Concrete					
Damage Constant, D1	4.00E-02	4.00E-02	4.00E-02	4.00E-02	4.00E-02
Damage Constant, D2	1.00	1.00	1.00	1.00	1.00
Minimum Strain to Failure	1.00E-02	1.00E-02	1.00E-02	1.00E-02	1.00E-02
Residual Shear Mod Fraction	1.30E-01	1.30E-01	1.30E-01	1.30E-01	1.30E-01
Tensile failure	Principal stress	Principal stress	Principal stress	Principal stress	Principal stress
Principal stress lim σ_{1lim} (MPa)	12	15.8	17.4	17.4	60.0
Fracture energy (N/m)	120	150	200	200	600

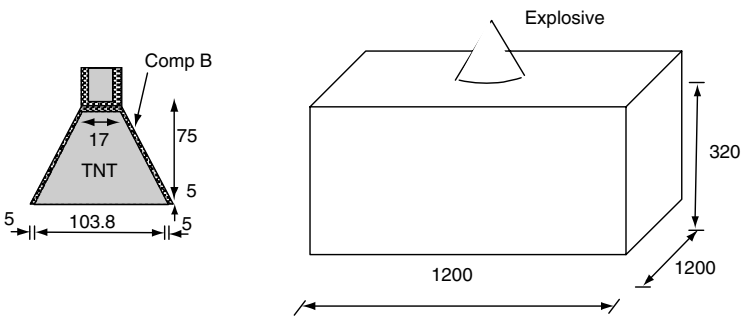

Figure 1. Test layout (Dimensions in mm) (11)

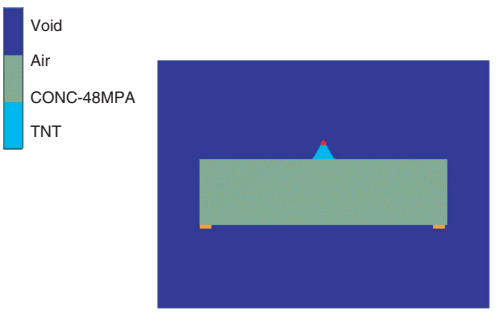

Figure 2. Numerical model for the slab

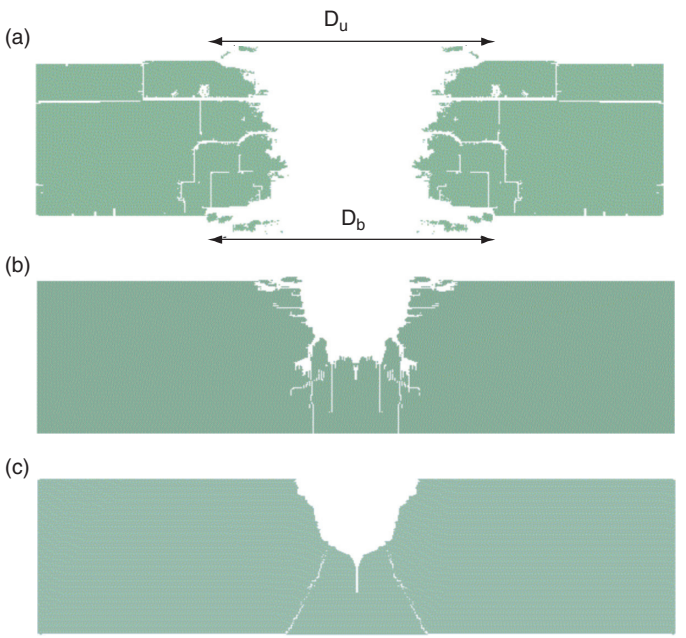

Figure 3. Damaged slab (Numerical simulation for a 2 mm mesh size) for different erosion limits. (a) $(\varepsilon_{eff})_{lim}$ = 0.001; (b) $(\varepsilon_{eff})_{lim}$ = 0.01; (c) $(\varepsilon_{eff})_{lim}$= 0.1

Table 3. Summary of experimental and numerical results for crater dimensions

Results		**Upper crater diameter (mm)**	**Bottom crater diameter (mm)**
Test [11]		510	620
Numerical			
Mesh size (mm)	Erosion criteria and limit		
2	$\left(\varepsilon_{eff}\right)_{\lim} = 0.001$	520	570
2	$\left(\varepsilon_{eff}\right)_{\lim} = 0.01$	370	——
2	$\left(\varepsilon_{eff}\right)_{\lim} = 0.1$	240	——
10	$\left(\varepsilon_{eff}\right)_{\lim} = 0.0002$	560	720
2	$\left(\sigma_1\right)_{\lim} = 10$ MPa	620	620

Figure 4. Damaged slab (Numerical simulation 10 mm mesh size). $(\varepsilon_{\text{eff}})\text{lim} = 0.0002$

The results obtained using a 2 mm mesh size for the plate and a plastic strain based erosion criterion taking $\left(\varepsilon_{eff}^{p}\right)_{\lim} = 0.001$ are coincident with those obtained with effective strain criterion and the same limit presented in Figure 3b and Table 3. Elastic extension of concrete is small when compared to plastic strain so the difference between total strain and plastic strain practically does not affect the final erosion.

The results obtained using a 2 mm mesh size for the plate and an erosion criterion based on maximum principal stress are presented in Figure 5 and Table 3. To model this criterion, principal stress $\left(\sigma_1\right)_{\lim} = 10$ MPa was used to model tensile failure (Table 2) and erosion based on failure was defined. It can be seen that the numerical model approximately reproduces the damage observed in the experiment. Nevertheless the shape of the perforation was better reproduced using a strain based erosion criteria.

The same problem was simulated with a 2mm mesh size and an erosion criterion based on failure defined by RHT model. The erosion observed in the test could not be reproduced using the default values for the parameters describing damage. When the parameters defining the fracture surface were modified, the resulting crater was enlarged but physical erosion observed in the test could not be reproduced.

Figure 5. Damaged slab (Numerical simulation 2 mm mesh size) $\sigma_1 \geq (\sigma_1)$ lim

The problem was also solved with a 2 mm mesh size and an erosion criterion based on failure defined by $p_{\min} = 0$. Actual erosion could not be reproduced using this criterion.

3.3. RECTANGULAR REINFORCED CONCRETE PLATE UNDER BLAST LOAD (40)

The numerical simulation of the reinforced concrete slab tested by Wu *et al*.. [40] under explosive loading in a blast chamber is presented in this section. The scabbing hole formed was compared with that obtained in the test.

The dimensions of the slab and the reinforcement are indicated in Figure 6. The specimen was reinforced on both faces. Concrete and steel properties are presented in Table 2 and 4 respectively. The slab was simply supported at its shorter sides and it was subjected to an equivalent of 2.09 kg of TNT at a standoff distance of 0.6 m.

The detonation of the explosive load was first simulated with the axial symmetric model shown in Figure 7a consisting of an Euler Gudunov mesh. A cylindrically shaped explosive with a radius to length ratio of 1:1 and vertical axis was modeled. In a second step, the results obtained with this first model were mapped on the 3D model shown in Figure 7b that includes the plate and the surrounding air volume. The plate was modeled with 3D elements of 2.5 mm side and the reinforcement was simulated as steel bars. Although the complete slab is shown in Figures 7c and 7d, considering the problem symmetry, only the fourth plate was modeled.

RHT model was used for concrete and an elastoplastic model for the steel bars. The material properties presented in Tables 2 and 4 were used. Different erosion criteria for

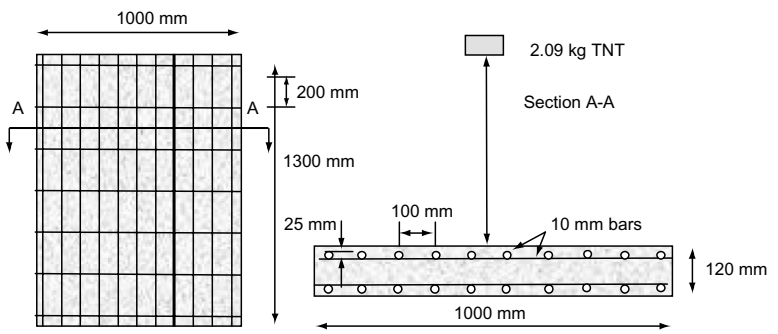

Figure 6. Reinforced concrete slab under blast load (40)

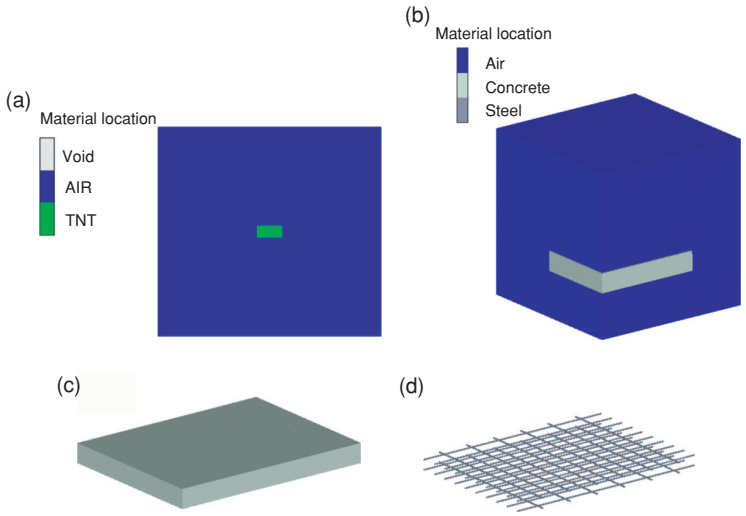

Figure 7. Numerical model for Wu *et al.* (40) blast experiment. (a) Detonation of the explosive load; (b) Reinforced concrete plate and surrounding air volume (one fourth); (c) Reinforced concrete plate; (d) Reinforcement

Table 4. Steel properties

Material properties	**Application example, section**		
	3.3	**3.4**	**3.5**
Young Modulus (GPa)	200	200	200
Yield stress (MPa)	560	— —	— —
Ultimate strength (MPa)	605	600	600

concrete were tested in this problem. It was no possible to reproduce experimental results with an erosion criterion based on strains. The best results were achieved with an erosion criterion based on maximum principal stress. Considering the strain rate strength enhancement, a stress limit equal to 3 times the tension strength of concrete was used. The final state of the plate numerically obtained is shown in Figure 8. Additionally, the dimensions of the scabbing hole numerically obtained are compared with experimental results in Table 5. A good correlation between numerical and experimental results was found for the erosion criterion and limit used.

The same problem was solved using a 5 mm and 10 mm side meshes for the slab and the same erosion criterion and limit to study the dependence on mesh size. The dimensions of the scabbing hole were similar to those obtained with the 2.5 mm mesh, showing the independence on mesh size. However, the damage zone was better reproduced by the finest mesh. All the simulations performed for this slab showed concrete failure near the reinforcement that was not observed in the test and that can be attributed to the interaction algorithm between solid and bar elements. This effect was reduced as the mesh was refined.

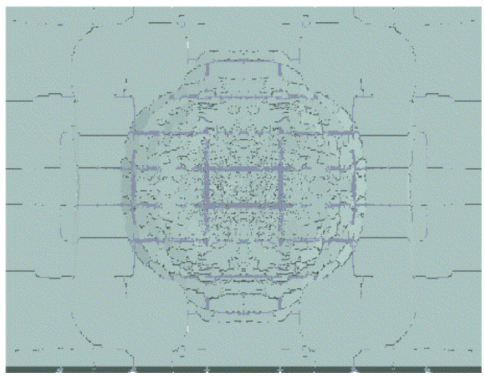

Figure 8. Scabbing hole. Numerical simulation

Table 5. Scabbing hole data

Material	Max. length (mm)	Max. width (mm)	Max. depth (mm)
Test [40]	600	570	65
Numerical (2.5 mm)	610	580	70

3.4. SQUARE REINFORCED CONCRETE SLABS UNDER BLAST LOAD (41)

The numerical simulation of square reinforced concrete slabs tested by Wang *et al*. [41] under blast loads at different scaled distances are presented in this section. The dimensions of the slabs and the reinforcement are shown in Figure 9. The slabs were clamped down on two opposite sides and subject to cylindrical explosive charges consisting of 0.64 and 0.94 kg of TNT suspended at a standoff distance of 500 mm. The diameter-to-height ratio of the explosive charge was approximately two. The material properties presented in Tables 2 and 4 were used for concrete and steel respectively.

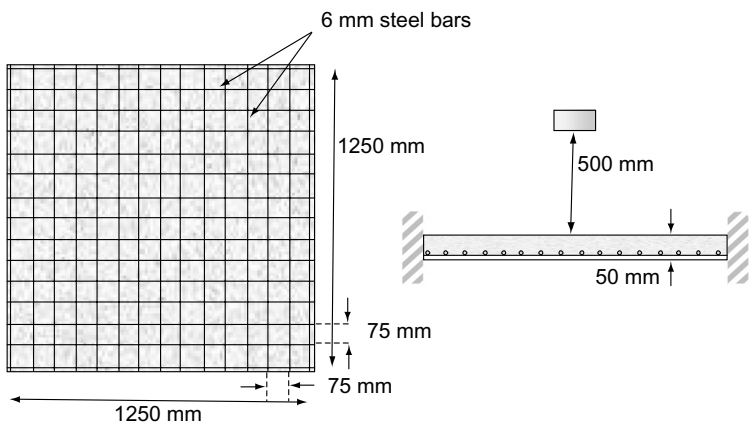

Figure 9. Reinforced concrete slabs under blast load at different standoff distances (41)

The numerical model used to simulate this problem is presented in Figure 10. First the detonation of the cylindrical explosive charge was simulated in an axial symmetric model consisting of the explosive and the surrounding air volume. Then, the results were mapped on the 3D model shown in Figure 10a consisting of the reinforced concrete slab and the surrounding air volume. Due to the symmetry of the problem only one fourth of the slab was actually modeled using 3.125 mm side cells.

Different erosion criteria and erosion limits for concrete were tested in this problem. The best results were achieved with an erosion criterion based on maximum principal stress with a stress limit equal to 4 times the tension strength of concrete. The experimental results were also approximately reproduced with an erosion criterion based on instantaneous geometric strains with a limit of 0.005.

The numerical results obtained with both erosion criteria for the two different amounts of explosive loads analyzed and their comparison with experimental results are presented in Figures 11 and 12 and Table 6 where the dimensions of the scabbing hole and maximum slab deflection are consigned.

It can be observed that experimental results are approximately reproduced using a both criteria but concrete spalling in back face is not reproduced. As in the previous problem, concrete surrounding the reinforcement is more damaged than in the tests.

3.5. REINFORCED CONCRETE AND ULTRAHIGH PERFORMANCE FIBER REINFORCED SLABS UNDER BLAST LOADS (42)

The numerical simulation of reinforced concrete and ultrahigh performance fiber concrete (UHPFC) slabs tested by Wu *et al*. [42] under blast loads is presented in this section. The tests numerically simulated are described in Table 7. The dimensions of the slabs and reinforcement are shown in Figure 13. All the slabs, except for that called UHPFC, were reinforced with steel bars.

The specimens were tested on a steel frame with an effective span of 1800 mm. The explosive charges were cylindrical with horizontal axis and a diameter to length ratio of 1:1. The mechanical properties of the materials are presented in Tables 2 and 4.

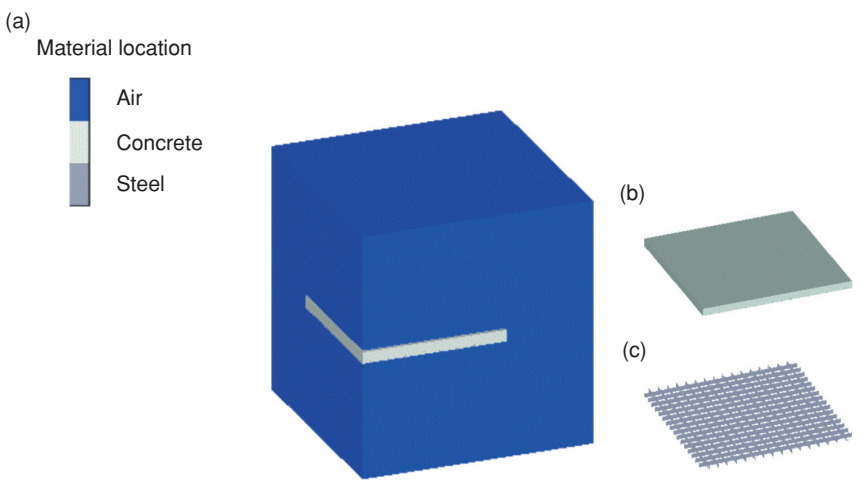

Figure 10. Numerical model for Wang *et al.* (41) blast experiment. (a) Reinforced concrete slab and surrounding air volume (one fourth); (b) Reinforced concrete slab; (c) Reinforcement

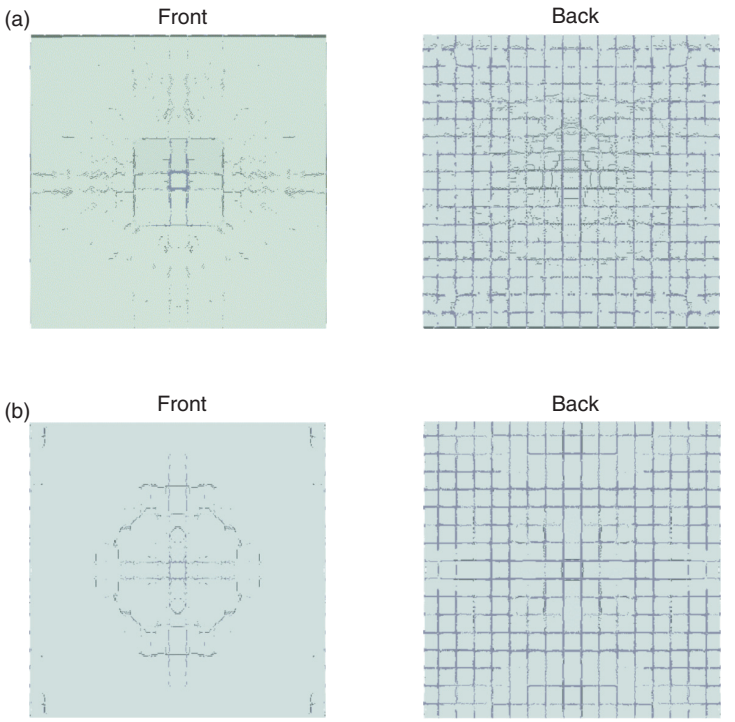

Figure 11. Scabbing holes obtained in front and back faces (0.64 kg TNT). Numerical simulation. a) Erosion criterion: maximum tensile stress $(\sigma_1)_{lim} = 4f_t$; b) Erosion criterion: instantaneous geometric strain $(\varepsilon_{eff})_{lim} = 0.005$

This problem was simulated in two steps. First, the detonation of the explosive and the first instants of shock wave propagation were simulated in axial symmetric models. Then, the results of these problems were mapped on 3D models consisting of the slab and the surrounding air volume as that presented in Figure 14. In the tests, the explosive load was detonated from one of the ends of the cylinder and not from the center, so the problem was not exactly symmetric with respect to two axes. Nevertheless, it was assumed symmetric for the numerical simulation. Accordingly, only one fourth of the slab was simulated with 16.67 mm cells. RHT model was used both for concrete and UHPFC but different properties (see Table 2) were used for them. An erosion criterion based on maximum stress with and erosion limit of four times the static tensile strength was used in both cases. Steel was modeled with a classical plasticity model with the properties presented in Table 4.

To check the ability of the numerical model to reproduce the blast wave, the pressure time histories in point PT1 (Figure 13) were registered. The peak side on overpressures, the peak reflected overpressure and peak reflected impulse values are compared with available experimental results in Table 8. It can be observed the numerical models reproduced experimental values with reasonable accuracy except for the case of pressure values in tests NRC-1 and NCR-2. Similar differences were found for this case by Wu *et al.* [42] when they predicted the peak overpressure values with TM5 [43].

Additionally, the maximum deflections of the slabs numerically obtained are compared with those measured in the tests in Table 8. In general, a good agreement between experimental and numerical results was found. In correspondence with pressure results, the

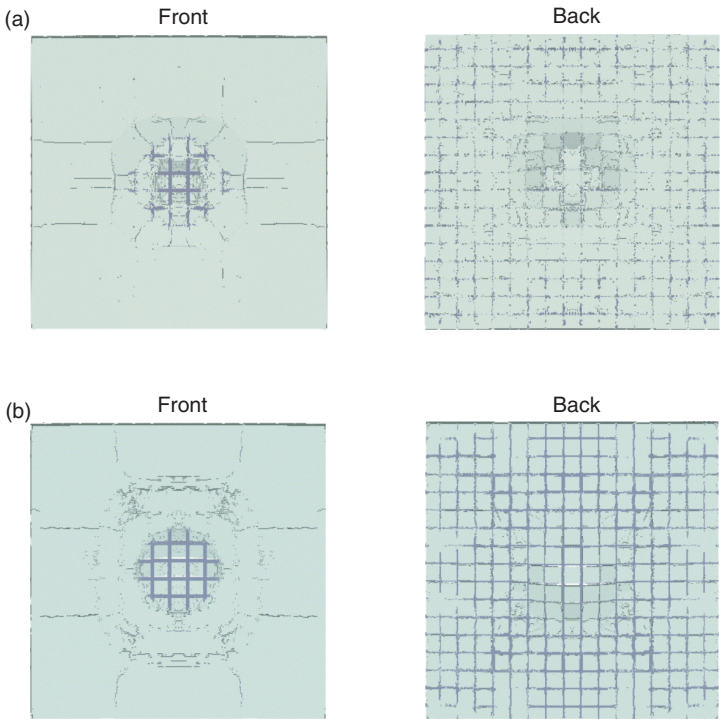

Figure 12. Scabbing holes obtained in front and back faces (0.94 kg TNT). Numerical simulation. a) Erosion criterion: maximum tensile stress $(\sigma_1)_{lim} = 4ft$; b) Erosion criterion: instantaneous geometric strain $(\sigma_{eff})_{lim}$

Table 6. Damage data. Comparison of experimental (41) and numerical results

Explosive	Central deflection (mm)			Spall radius (mm)		
		Numerical			Numerical	
(kg TNT)	Test	$(\sigma_1)_{lim}$	$(\varepsilon_{eff})_{lim}$	Test	$(\sigma_1)_{lim}$	$(\varepsilon_{eff})_{lim}$
0.64	19	30	27	120	190	118
0.94	40	40	36	185	194	187

Table 7. Experimental program (42)

Specimen	Material	Standoff distance (m)	Explosive mass (kg TNT)	Scaled distance (m/kg$^{1/3}$)
NRC-1	RC	3.0	1.007	3.00
NRC-2	RC	3.0	8.139	1.50
NRC-3	RC	1.4	3.440	0.93
UHPFC	UHPFC	0.75	3.433	0.50
RUHPFC	RUHPFC	1.00	20.101	0.37

RC: reinforced concrete, UHPFC: ultra high performance fibrous concrete, RUHPFC: reinforced ultra high performance fibrous concrete

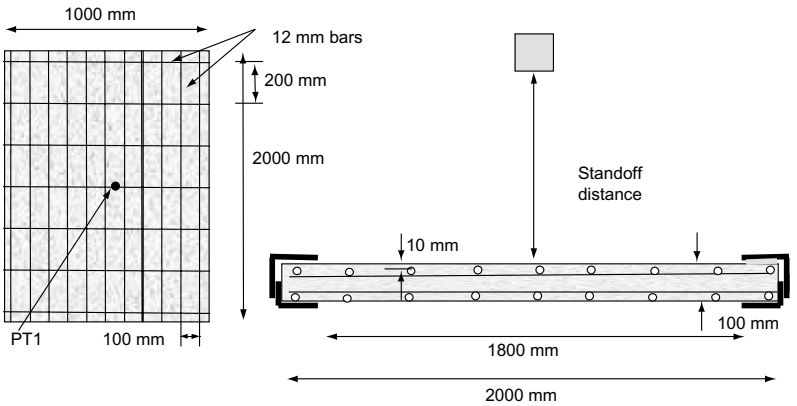

Figure 13. Slabs dimensions, reinforcement and supports (42)

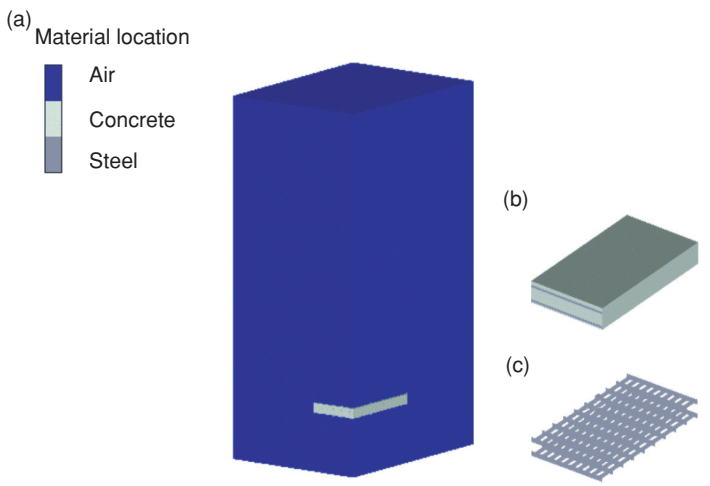

Figure 14. Numerical model for Wu *et al.* (42) blast experiment. (a) Reinforced concrete slab and surrounding air volume (one fourth), (b) Reinforced concrete slab; (c) Reinforcement

Table 8. Blast pressure and maximum displacements. Comparison of numerical and experimental results (42)

Specimen	**Peak side on overpressure PT1 (MPa)**		**Peak reflected overpressure PT1 (MPa)**		**Peak reflected impulse PT1 (MPa ms)**		**Max. deflection (mm)**	
	Test	**Numer.**	**Test**	**Numer.**	**Test**	**Numer.**	**Test**	**Numer.**
NRC-1	0.13	0.07	0.42	0.21	0.186	0.153	1.5	1.5
NRC-2	0.54	0.35	2.39	1.65	0.715	0.752	10.5	5.7
NRC-3	1.43	1.17	6.38	7.53	0.705	0.721	13.9	15.6
UHPFC							13.2	12.50
RUHPFC							>100	>100

maximum deflection numerically obtained for slab NCR-2 was much lower than that obtained in the test.

4. CONCLUSIONS

A review of erosion algorithm frequently used in numerical simulations of blast and impact loading on concrete elements is presented. Erosion algorithms are numerical solutions to avoid great mesh deformation when Lagrange processors are used. Nevertheless, in the case of concrete they can be used to represent physical erosion, shear failure, cratering, spalling and fracture.

The review presented shows a great dispersion of erosion criteria and erosion limits used by different authors for similar types of concrete. The differences found suggest that erosion limit requires further research. The review also suggests that erosion criteria should be adequate to the type of "physical erosion" phenomena that is intended to be modeled.

Although very simple, erosion criteria based on strain and stress limits can be more easily related to physical phenomenon occurring in concrete under blast and impact loads. The examples developed show that the criterion based on instantaneous geometric strain is able to reproduce concrete failure under close blast loads but criterion based on maximum stress can also reproduce failure due to explosive loads at certain standoff distance. On the other side, concrete spalling is better simulated using a strain based erosion criterion.

From these results, a combination of instantaneous geometric strain limit and tensile stress limits represents an adequate erosion criterion to reproduce different types of concrete failure under blast loads. Moreover, it should be observed that a very fine mesh must be used to obtain the shape of the damaged zone registered in tests under contact or close blast loads. This is not the case of more distant explosions characterized by flexure failure that can be modeled with coarser meshes.

The comparison with experimental results proves that erosion limit based on strain limits is not independent of mesh size, thus it cannot be considered as a material property. Different results are normally expected to be obtained when the same problem is solved with different mesh sizes. Nevertheless, the difference tends to disappear when the mesh is refined. If strain based erosion criteria is considered, another type of mesh size dependency is introduced in the numerical solution. A simple correlation between mesh size and erosion limit is used in the paper to obtain similar numerical results. However, this dependency requires further research in order to establish the range of validity and if there are not other variables influencing this problem.

The limits used for tensile stress should take into account the strength enhancement due to strain rate. Nevertheless, while strain rate decreases with the scaled distance, the application examples and comparison with experimental results developed showed that the tensile stress limit should be increased with scaled distance. This effect can be attributed to the fact that different phenomena are actually modeled with the same algorithm, so the stress limit represents different strength thresholds.

It is evident from numerical results in Section 3.5 that there are certain inaccuracies in the blast pressure numerical simulations. It is important to know this fact when trying to reproduce damage. Another source of discrepancy between numerical and experimental results can also be attributed to the Euler-Lagrange interaction.

AKNOWLEDGEMENTS

The financial support of the CONICET (Argentina) and CIUNT (National University of Tucumán) and the collaboration of Ms. Amelia Campos in the English revision are gratefully acknowledged.

REFERENCES

[1] Alia, A. and Souli M., High Explosive Simulation Using Multi-Material Formulations, *Applied Thermal Engineering*, 2006, 26,1032–1042.

[2] Hargather, M.J. and Settles, G. S., Laboratory-Scale Techniques for the Measurement of a Material Response to an Explosive Blast, *International Journal of Impact Engineering*, 2009, 36, 940–947.

[3] Sorensen, A. and McGill, W., Review. What to Look for in the Aftermath of an Explosion? A Review of Blast Scene Damage Observables, *Engineering Failure Analysis*, 2011, 18, 836–845.

[4] Ambrosini, R.D., Luccioni, B.M. ‚Jacinto, A. and Danesi, R., Location and Mass of Explosive from Structural Damage, *Engineering Structures*, 2005, 27(2), 167–176.

[5] Luccioni, B., Ambrosini, R.D. and Danesi, R., Predicting the Location and Size of Explosive Device Detonated in an Urban Enviroment Using Evidence from Building Damage, *Proceedings of the Institution of Civil Engineers, Structures & Buildings*, 2005, 158(SB1), 1–12.

[6] Remennikov, A. and Rose, T., Predicting the effectiveness of blast wall barriers using neural networks, *International Journal of Impact Engineering*, 2007, 34(12), 1907–1923.

[7] Lian, Y.P., Zhang, X., Zhou, X. and Ma, Z. T., A FEMP Method and its Application in Modeling Dynamic Response of Reinforced Concrete Subjected to Impact Loading, *Computer Methods Applied Mechanics and Engineering, 2011,* 200, 1659–1670.

[8] Millard, S., Molyneaux, T., Barnett, S. and Gao, X., Dynamic Enhancement of Blast-Resistant Ultra High Performance Fibre-Reinforced Concrete under Flexural and Shear Loading, *International Journal of Impact Engineering*, 2010, 37, 405–413.

[9] Burlion, N., Gatuingt, F., Pijaudier-Cabot, G. and Daudeville, L., Compaction and Tensile Damage in Concrete: Constitutive Modelling and Application to Dynamics, *Computer Methods Applied Mechanics and Engineering*, 2000, 183, 291–308.

[10] Unosson, M., *Constitutive Equations for Concrete Materials Subjected to High Rate of Loading*. *Linköping Studies in Science and Technology*. Thesis No. 936. LIU-TEK-LIC-2002:09. Department of Mechanical Engineering. Division of Solid Mechanics. Linköpings universitet. Linköping, Sweden, 2002.

[11] Rabczuk, T. and Eibl, J., Modelling Dynamic Failure of Concrete with Meshfree Methods, *International Journal of Impact Engineering*, 2006, 32, 1878–1897.

[12] Tu, Z. and Lu, Y., Evaluation of Typical Concrete Material Models Used in Hydrocodes for High Dynamic Response Simulations, *International Journal of Impact Engineering*, 2009, 36, 132–146.

[13] Tu, Z. and Lu, Y., Modifications of RHT Material Model for Improved Numerical Simulation of Dynamic Response of Concrete, *International Journal of Impact Engineering*, 2010, 37, 1072–1082.

[14] Zhou, X.Q. and Hao, H., Mesoscale Modelling and Analysis of Damage and Fragmentation of Concrete Slab under Contact Detonation, *International Journal of Impact Engineering*, 2009, 36, 1315–1326.

[15] Riedel, W., Mayrhofer, C., Thoma, K. and Stolz, A., Engineering and Numerical Tools for Explosion Protection of Reinforced Concrete, *International Journal of Protective Structures*, 2010, 1(1), 85–101.

[16] Tai, Y.S., Chu, T.L., Hu, H.T. and Wu, J.Y., Dynamic Response of a Reinforced Concrete Slab Subjected to Air Blast Load, *Theoretical and Applied Fracture Mechanics*, 2011, 56, 140–147.

[17] Wang, W., Zhang, D., Lu, F., Wang, S. and Tang, F., Experimental Study and Numerical Simulation of the Damage Mode of a Square Reinforced Concrete Slab under Close-in Explosion, *Engineering Failure Analysis*, 2013, 27, 41–51.

[18] Zukas, J., *Introduction to hydrocodes*. Studies in applied mechanics (Elsevier) 49, 2004.

[19] Wu, K-C., Li, B. and Tsai, K-C., The Effects of Explosive Mass Ratio on Residual Compressive Capacity of Contact Blast Bamaged Composite Columns, *Journal of Constructional Steel Research*, 2011, 67, 602–612.

[20] ANSYS AUTODYN. *Interactive Non-Linear Dynamic Analysis Software*, Version 12, User's Manual. SAS IP Inc., 2009.

[21] Nyström, U. and Gylltoft, K., Numerical Studies of the Combined Effects of Blast and Fragment Loading, *International Journal of Impact Engineering*, 2009, 36, 995–1005.

[22] Hao, Y., Hao, H. and Li, Z-X., Confinement Effects on Impact Test of Concrete Compressive Material Properties, *International Journal of Protective Structures*, 2010, 1(1), 145–167.

[23] Beppu, M., Miwa, K., Itohb, M., Katayama, M. and Ohno, T., Damage Evaluation of Concrete Plates by High-Velocity Impact, *International Journal of Impact Engineering*, 2008, 35, 1419–1426.

[24] Riedel, W., Kawai, N. and Kondo, K-I., Numerical Assessment for Impact Strength Measurements in Concrete Materials, *International Journal of Impact Engineering*, 2009, 36, 283–293.

[25] Islam, J., Liu, Z. and Swaddiwudhipong, S., Numerical Study on Concrete Penetration/Perforation under High Velocity Impact by Ogive-Nose Steel Projectile, *Computers and Concrete*, 2011, 8(1), 111–123.

[26] Nyström, U. and Gylltoft, K., Comparative Numerical Studies of Projectile Impacts on Plain and Steel-Fibre Reinforced Concrete, *International Journal of Impact Engineering*, 2011, 38, 95–105.

[27] Shi, Y., Li, Z-H. and Hao, H., A New Method for Progressive Collapse Analysis of RC Frames under Blast Loading, *Engineering Structures*, 2010, 32, 1691–1703.

[28] Tang, E.K.C. and Hao, H., Numerical Simulation of a Cable-Stayed Bridge Response to Blast Loads, Part I: Model Development and Response Calculations, *Engineering Structures*, 2010, 32, 3180–3192.

[29] Wang, Z.L., Wu, J. and Wang, J.G., Experimental and Numerical Analysis on Effect of Fibre Aspect Ratio on Mechanical Properties of SRFC, *Construction and Building Materials*, 2010, 24, 559–565.

[30] Xu, K. and Lu, Y., Numerical Simulation Study of Spallation in Reinforced Concrete Plates Subjected to Blast Loading, *Computers and Structures*, 2006, 84, 431–438.

[31] Wang, Z.L., Konietzky, H. and Huang, R.Y., Elastic–Plastic-Hydrodynamic Analysis of Crater Blasting in Steel Fiber Reinforced Concrete, *Theoretical and Applied Fracture Mechanics*, 2009, 52, 111–116.

[32] Teng, T., Chu, Y., Chang, F., Shen, B. and Cheng, D., Development and Validation of Numerical Model of Steel Fiber Reinforced Concrete for High-Velocity Impact, *Computational Materials Science*, 2008, 42, 90–99.

[33] Farnam, Y., Mohammadi, S. and Shekarchi, M., Experimental and Numerical Investigations of Low Velocity Impact Behaviour of High-Performance Fiber-Reinforced Cement Based Composite, *International Journal of Impact Engineering*, 2010, 37, 220–229.

[34] Coughlin, A.M., Musselman, E.S., Schokker, A.J. and Linzell, D.G., Behavior of Portable Fiber Reinforced Concrete Vehicle Barriers Subject to Blasts from Contact Charges, *International Journal of Impact Engineering*, 2010, 37, 521–529.

[35] LS-DYNA *Keyword user's manual*, Version 970. Livermore Software Technology Corporation, 2003.

[36] Aráoz, G.F. and Luccioni, B.M. , Curva de Fragilidad para Muro de Mampostería bajo Cargas Explosivas a partir de Simulaciones Numéricas, *XX Jornadas Argentinas de Ingeniería Estructural*, 2008.

[37] Lee, E.L. and Tarver, C.M., Phenomenological Model of Shock Initiation in Heterogeneous Explosives, *Physics of Fluids*, 2008, 23(12), 2362–2372.

[38] Riedel, W., Thoma, K. and Hiermaier, S. , Numerical Analysis Using a New Macroscopic Concrete Model for Hydrocodes, *Proc. 9th Int. Symposium on Interaction of effects of Munitions with Structures*, 1999, 315–22.

[39] Herrmann, W., Constitutive Equation for the Dynamic Compaction of Ductile Porous Materials, *Journal Applied Physics*, 1969, 40(6), 2490–2499.

[40] Wu, C., Nurwidayati, R. and Oehlers, D. J., Fragmentation from Spallation of RC slabs Due to Airblast Loads, *International Journal of Impact Engineering*, 2009, 36, 1371–1376.

[41] Wang, W., Zhang, D., Lu, F., Wang, S-C. and Tang, S-C., Experimental Study on Scaling the Explosion Resistance of a One-Way Square Reinforced Concrete Slab under a Close-in Blast Loading, *International Journal of Impact Engineering*, 2012, 49, 158–164.

[42] Wu, C., Oehlers, D.J., Rebentrost, M., Leach, J. and Whittaker, A.S., Blast Testing of Ultra-High Performance Fibre and FRP-Retrofitted Concrete Slabs, *Engineering Structures*, 2009, 31, 2060–2069.

[43] TM5-855-1. *Fundamental of protective design for conventional weapons*. US Army Engineer Waterways Experiment Station, Vicksburg; 1984.